JOURNAL OF MATERIALS SCIENCE 25 (1990) 4518–4524

Particle coarsening kinetics during thermal decompositions: CdO from $CdCO_3$

J. R. SCHOONOVER, S. H. LIN
Department of Chemistry, Arizona State University, Tempe, Arizona 85287-1604, USA

In situ synchrotron X-ray diffraction determination of product particle size during the thermal decomposition of $CdCO_3$ powders is evaluated for sintering kinetics. The rate-determining step for particle growth is not the same during the reaction as after, the data suggesting surface diffusion during decomposition but evaporation–condensation after. Reasons for the difference are discussed, including the parent-phase matrix and CO_2 from the decomposition. When compared with loss of crystal imperfections, four stages of growth are seen, each affecting the reactivity of the product.

1. Introduction

The thermal decomposition of metal salts to their oxide has long been used to synthesize oxides for use as catalysts or reagents. The chemical and physical properties of the active oxide, and hence its reactivity, depend upon the starting material and the decomposition path. During the decomposition both reactant and product undergo annealing and sintering. The consequences include decreased interfacial contact with a second phase through surface-area reduction, decreased diffusivity of surface-absorbed molecules into the bulk, or decreased diffusivity from another solid phase; in all cases the movement of the reaction interface may be retarded. In addition, there may be an effect on the reversibility of a decomposition, which may account for the failure of rate laws near the end of the reaction and for isothermal retention.

In this paper, the coarsening kinetics of CdO during $CdCO_3$ decomposition is considered by *in situ* synchrotron X-ray diffraction. Both CdO and $CdCO_3$ are important catalysts, and the decomposition has been demonstrated as a path to novel oxides [1]. The method of *in situ* data collection, and the results obtained, are applicable to more widely considered systems of current interest, such as the decomposition of $BaCO_3$ during the synthesis of high-temperature ceramic superconductors. The completion of this reaction is severely delayed with the increase in BaO particle size by sintering at reaction temperatures [2].

The *in situ* diffraction experiments were performed from 649 to 700 K [3]. The X-ray diffraction profiles were analysed as a function of time for particle size and imperfections. The kinetics for particle growth during reaction were fitted to the equation

$$1 - \frac{r(t)}{r_f} = Ae^{-kt} \quad (1)$$

where $r(t)$ is the particle size at time t, r_f is the maximum particle size obtained during reaction, and A and k are constants [3]. This equation is characteristic of solutions for precipitation reactions and for diffusion from spheres and sheets

$$1 - \alpha(t) = \sum_{n=1}^{\infty} A_n e^{-Da_n t} \quad (2)$$

where D is the diffusion coefficient and A_n and a_n are constants involving n and are dependent on the geometry and boundary conditions. If a_n is large, this reduces to Equation 1. For growth after reaction, the data were fitted to a linear equation, which failed at the end of the reaction unless that equation is an approximation of Equation 1 for small kt and for which r_f is not known from the available data. A determination of activation energies showed that they were similar during and after reaction (~ 155 kJ mol^{-1}), the rate constants differing through the pre-exponential factor by two orders of magnitude. The difference in rate constants was accounted for by change in imperfection density with annealing. We have also found that Equation 1 may be fitted to Nan's results for growth during $MgCO_3$ calcination [4]. We have derived Equation 1 for a model of concomittant chemical reaction and product recrystallization [5].

However, because Equation 1 does not account for the induction period, nor the broad plateau in growth that begins just before and continues until just after the reaction, as well as because CdO, owing to its high vapour pressure, easily undergoes coarsening [6], and sintering during decompositions is common, we will consider here particle growth during reaction to be by coarsening with the usual rate law

$$\frac{dr(t)}{dt} = kr(t)^{n-1} \quad (3)$$

and

$$r^n(t) - r^n(t_0) = k(t - t_0) \quad (4)$$

where n depends on the mechanism of mass transport. For plastic flow, $n = 1$, for volume diffusion, $n = 2$, for evaporation–condensation, $n = 3$, and for surface diffusion, $n = 4$. More than one mechanism of mass

0022–2461/90 $03.00 + .12

transport may be operating, in which case Equation 4 becomes a polynomial. For a given sintering mechanism, more than one mechanism of mass transport may be involved, although one mechanism may be rate determining [7].

2. Experimental procedure and analysis

The high-temperature powder X-ray diffraction data were collected at the Stanford Synchrotron Radiation Laboratory (SSRL) at an eight-pole wiggler side-station with an unfocused silicon (220) monochrometer tuned at 8.0 keV. The sample was heated with a wrap-around radiation furnace. The specimen temperature was calibrated to the furnace temperature measured during an experiment prior to the experiments. All runs were in air. Data collection was by step scanning a germanium detector at 0.030° 2θ intervals with a 1 to 2 sec dwell. During the reaction, the detector was oscillated continuously over the parent or product profile of interest, giving a collection time per profile of $\frac{1}{2}$ to 1 min, depending on the desired counting statistics, the extent of the tails included, the rate of reaction, and whether only a product-phase profile was monitored or a profile from each phase.

The data were analysed whenever practical with the variance-range equation [8, 9]

$$w(\sigma) = k\sigma + w_0 \tag{5}$$

where $w(\sigma)$ is the variance determined over σ, the distance in 2θ or Q from the profile peak. k is related to the particle size through

$$K = \frac{\lambda k_w}{2\pi^2 p \cos\theta} \tag{6}$$

where k_w is the Scherrer constant, λ the wavelength, and p the particle size. w_0 is related to particle size and imperfection. For strain broadening

$$w_0 = -\frac{\lambda^2 L}{4\pi^2 p^2 \cos\theta} + \langle e^2 \rangle \tan^2\theta \tag{7}$$

where L is the taper parameter and $\langle e^2 \rangle$ is the variance of the strain. The profile variance and the fit to Equation 5 were determined iteratively using Langford and Wilson's method [10]. Instrumental broadening

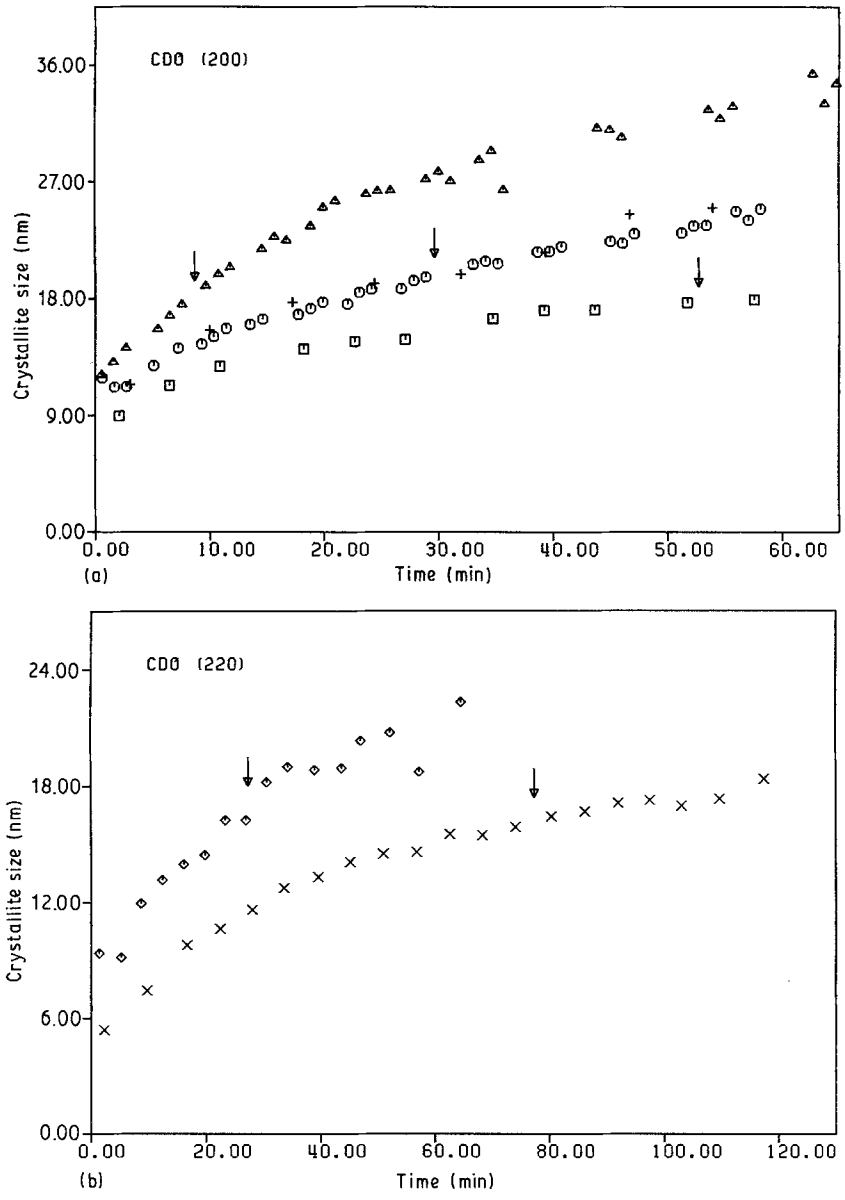

Figure 1 CdO crystallite size as a function of calcination and sintering time. The imperfection profile broadening has not been removed. The arrows indicate the end of the reaction. (□) CdO (200), 655 K; (○) CdO (200), 675 K; (△) CdO (200), 700 K; (+) CdO (200), sample II, 675 K; (×) CdO (220), 649 K; (◇) CdO (220), 675 K.

and truncation and nonadditivity corrections were applied to Equation 5 [8]. For spherical particles with negligible imperfection profile broadening, Equation 5 reduces to

$$w = \frac{\lambda k_w}{2\pi^2 p \cos\theta} \quad (8)$$

[11], which was applied to all profiles. Equation 8 is applied for cases where it is desirable to increase the number of time slices for statistical reasons, by decreasing the counting statistic or scan width, yet allowing a direct comparison with cases for which strain can be removed. The full width at half the maximum intensity (FWHM) gave similar kinetics to Equation 8, although the sizes were larger, as expected [12].

Only the CdO (2 2 0) and the CdO (2 0 0) lines are considered during the reaction, because for the other CdO profiles of acceptable intensity there is significant overlap with $CdCO_3$ lines. Particle growth after reaction is also considered for the CdO (1 1 1) plane. For comparison, crystallite growth during reaction of a second sample at 675 K is also considered.

3. Results and discussion

The product particle diameter as a function of time [3] shows a brief induction period before the onset of growth (Fig. 1). Growth continues until near the end of the reaction, after which there is a brief and sudden decrease in the rate to near zero. This is observed to occur before α, the extent of reaction, is one, except for temperatures at or above 700 K. For this case growth proceeds without interruption beyond $\alpha = 1$. After reaction, growth continues, but at a lower rate than during reaction. When strain broadening is removed, the induction period becomes more pronounced and for the CdO (2 2 0) profiles the growth plateau becomes considerably broadened (Fig. 2).

The particle growth during reaction for the two planes, CdO (2 2 0) and CdO (2 0 0), are not in agreement. Also, the CdO (1 1 1) profile does not show the same kinetics for CdO appearance as the other planes [3]. Data analysis by Equation 1 indicates that differences in the crystallite growth between the $[h\,k\,l]$ during reaction are strongly related to the initial particle shape. From Equation 1, the kinetics of growth may be fitted to a single Arrhenius plot.

The imperfection broadening rapidly decreases, becoming close to zero when the growth plateaus are reached [3]. The profiles show asymmetry early in the reaction that is characteristic of stacking faults.

In the discussion here, the data are first considered without removal of the profile strain broadening. This allows for an improvement in the time resolution so that high temperatures can be studied and better statistics for the size time dependence at low temperatures can be obtained. The results are then compared with the results for strain broadening removed.

The sintering exponent, n, may be determined through Herring's scaling laws [13] by a log–log plot, the slope of which is $1/n$ (Fig. 3). Three periods of growth are seen: (a) an induction period of very small slope, so that n is much greater than expected from conventional mass transport mechanisms for powder compacts; (b) growth during reaction, for which the average value of n is 4.4 ± 0.2, except for at 700 K at which $n = 6.2$; (c) post-reaction growth, for which the average value of n is 3.3 ± 0.1. In all cases, $1/n$ is determined by linear least squares.

It is expected that for the data without the removal of strain broadening, the slope of the log–log plots will be too low, and hence n too high. This is because CdO disorder is greatest early in the reaction, decreasing to near zero as the plateau in growth is reached [3]. However, if there is more than one mechanism of material transport operating, the apparent value of n may be too large and there may be nonlinearity.

There are two significant factors that may account for the induction period. (1) Early in the reaction the rate of formation of product particles by the reaction is greater than the rate of coarsening. Initially, the particle size distribution is determined by growth by activation, the particles fracturing at a critical particle size. (2) The parent-phase matrix limits contact between particles, as discussed below.

During the decomposition, the results best suggest

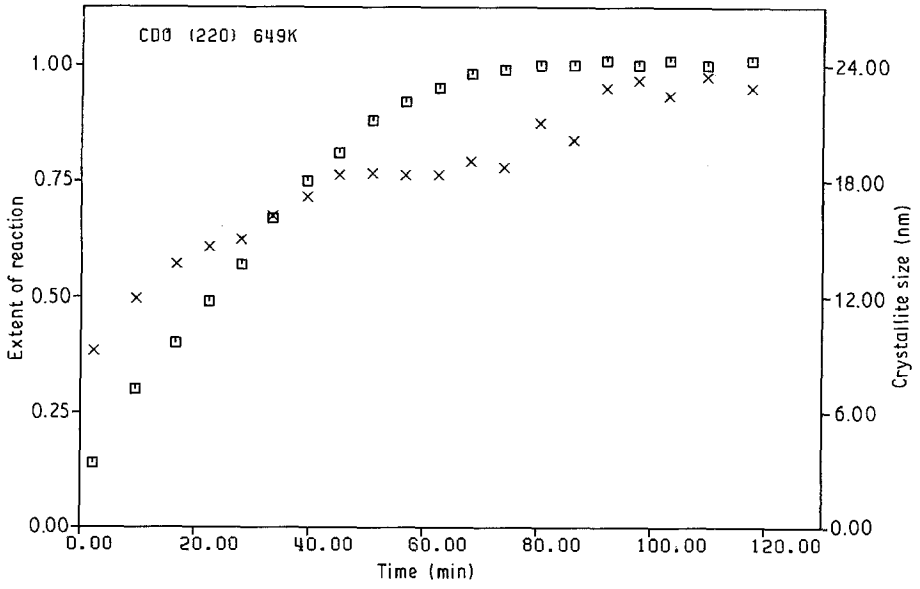

Figure 2 CdO (2 2 0) crystallite diameter as a function of time during the decomposition at 649 K after profile imperfection broadening has been removed (×) and the extent of reaction (□).

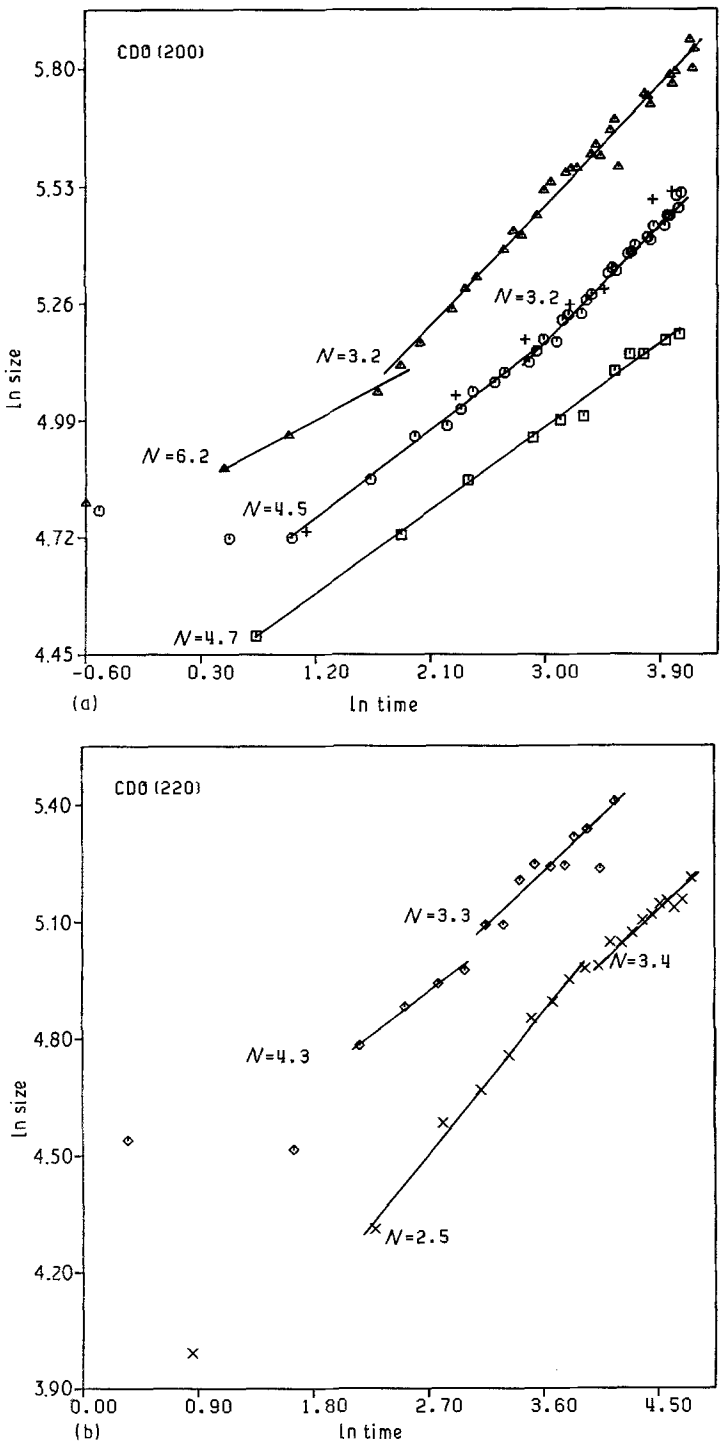

Figure 3 Log–log plots for coarsening of CdO from $CdCO_3$ decomposition before and after reaction as measured from (a) the CdO (200) and (b) CdO (220) high-temperature powder synchrotron X-ray diffraction profiles. The imperfection profile broadening has not been removed. For key see Fig. 1.

surface diffusion as the predominant material transport mechanism, so that

$$r^4(t) - r(t_0)^4 = k(t - t_0) \quad (9)$$

However, for high temperatures the value of n is ~ 6 from CdO (200). The only CdO (220) measurement at low temperature gave a very low value of 2.5; however, with removal of strain broadening, this value is in agreement with that for other data sets, as discussed below.

After reaction, the value of n strongly suggests evaporation–condensation kinetics

$$r(t)^3 - r(t_0)^3 = k(t - t_0) \quad (10)$$

Evaporation–condensation has been determined by Quadir and Ready [6] to be the likely material transport mechanism for the sintering of CdO particles several tenths of a micrometer in diameter at temperatures from 900 to 1100° C.

If surface diffusion is indeed the predominant coarsening mechanism during decomposition, then interconnectivity of the coarsening particles is significant. This suggests CdO aggregates are separated from one another by an unreacted parent-phase matrix. The matrix prevents contact of product nucleated in different sample regions, effectively preventing mass transport by surface diffusion in the early period of reaction, unless intra-aggregate porosity is relatively low. This results in the induction period. An intra-aggregate porosity significantly lower than inter-aggregate porosity has been observed during calcination [4, 14]. This is reasonable, because the CdO particles fracture during growth at a critical particle size [3]; they are initially, within the time resolution, at

most 10% of the diameter of the $CdCO_3$ particles. Therefore, a single $CdCO_3$ crystallite produces a cluster of CdO crystallites. Because surface diffusion is seen to begin early in the reaction, following a brief induction period, the CdO particles are forming from the parent particle within a short period relative to the time necessary for complete specimen decomposition. This autocatalysis can arise either from the reaction interface fracture that limits the initial product particle sizes by occurring behind the reaction boundary, or by stresses on the $CdCO_3$ side of the interface from the volume differentials, which will increase the nucleation frequency by introducing a strain energy.

It is not surprising that volume diffusion is not the rate-determining step because of the energy requirements in forming particle boundaries at the expense of surface area. However, volume diffusion may be the predominant mass transport mechanism, while the rate-determining step is the formation and development of necks [6]. This is the Greskovich–Lay mechanism [7].

The change in the rate-determining mass-transport mechanism from surface diffusion to evaporation–condensation can be attributed in part to the formation of necks. Following Kuczynski [15], the rate of neck volume change for two mechanisms operating simultaneously is

$$\frac{dV}{dt} = nf_{ev} + mf_s$$

$$\approx = \frac{2\pi}{r} X^2 \frac{dx}{dt} \quad (11)$$

where $n + m = 1$ and f_{ev} and f_s are the volume change rates for evaporation–condensation and surface diffusion, respectively. From Kuczynski [15]

$$f_{ev} = 4\pi \frac{KP}{\beta} \frac{\delta \to d^3}{kT} X \quad (12a)$$

$$f_s = 16\pi \frac{\delta \to d^3}{kT} D_s \frac{r^2}{X^3} \quad (12b)$$

where K is the evaporation rate constant, P the partial pressure, β a constant defined as $\beta\, dv/dt = AG$ (A is the neck area and G is the rate of evaporation), σ is the surface tension, d the interatomic distance, k Boltzmann's constant, D_s the surface diffusion coefficient, and X the neck diameter. The rate of neck growth is then

$$\frac{dx}{dt} = \frac{2a}{X^3} \frac{d^3}{kT} \left(n \frac{kP}{\beta} X + m^4 \frac{r^2}{X^3} D_3 \right) \quad (13)$$

From Equation 13, there are three factors that may shift the predominant mechanism of mass transport from surface diffusion to evaporation–condensation: (1) the relative rate of necking for surface diffusion decreases as $1/X^3$, while for evaporation–condensation it increases linearly with X; (2) the values of β and P for evaporation–condensation will tend to be time dependent. Initially the product CdO will be distributed randomly over the sample surface allowing poor CdO_g and Cd_g retention near the crystallite surfaces and a significant number of absorption sites in the sample will be on $CdCO_3$; (3) the surface diffusion coefficient may be greater in the presence of CO_2 through the formation of surface $CdCO_3$ on active CdO. CO_2 was found by Beruto *et al.* [16] to catalyse surface area reductions of CaO, and it has been reported that CO_2 promotes CdO growth during decomposition, although not necessarily after it [17]. Beruto *et al.* [16] speculated that CO_2 may promote surface reduction by enhancing surface diffusion. Also, the high density of imperfections, including stacking faults, of the active oxide will increase the diffusion coefficient.

With the removal of strain broadening, the kinetics in terms of particle coarsening are not as clear (Fig. 4). The growth as a function of time becomes more complex, the induction period and plateaus becoming more distinct, particularly for the (220) profile. Because the amount of strain after reaction is near zero and decreasing [3], the profile broadening is essentially from particle size; the conclusion of

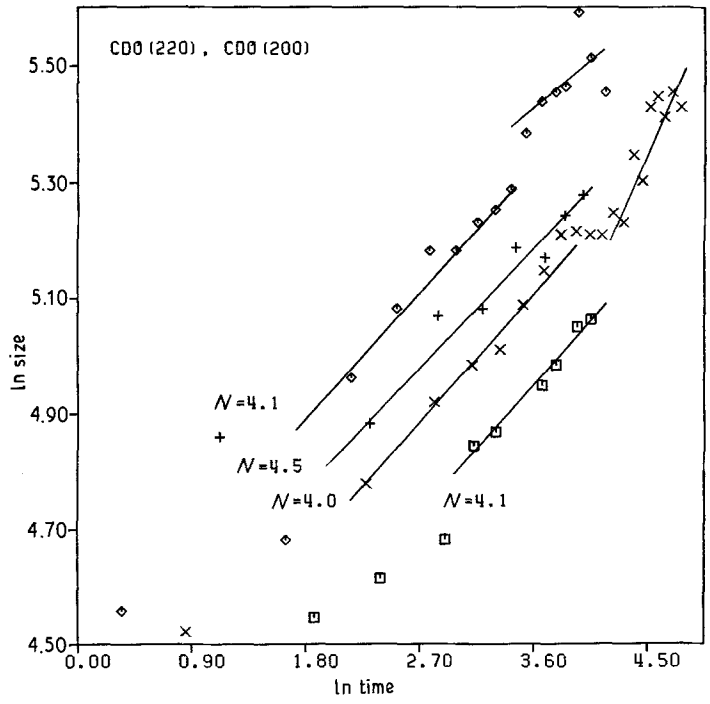

Figure 4 Log–log plots for coarsening of CdO from $CdCO_3$ decomposition before and after reaction as measured from the CdO (200) and CdO (220) high-temperature powder synchrotron X-ray diffraction profiles. Imperfection profile broadening has been removed. For key see Fig. 1.

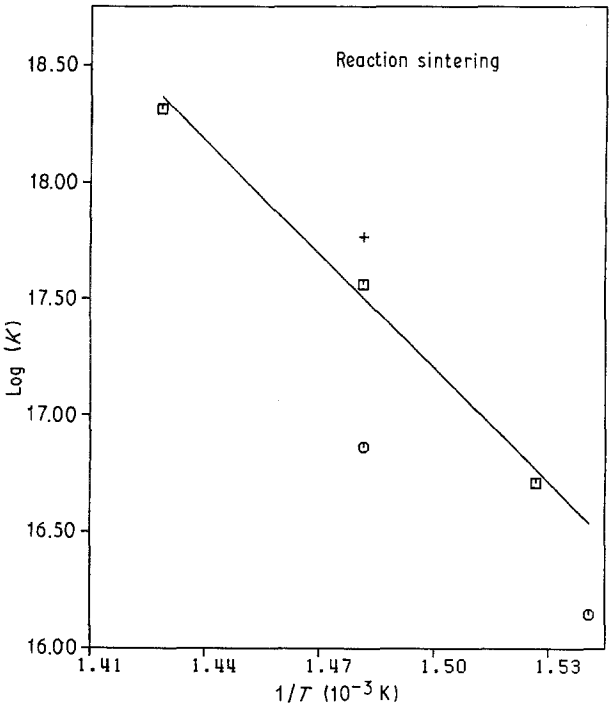

Figure 5 Arrhenius plot for the crystallite coarsening kinetics during reaction. Imperfection profile broadening has not been removed. (□) CdO (2 0 0), sample I; (○) CdO (2 2 0); (+) CdO (2 0 0), sample II.

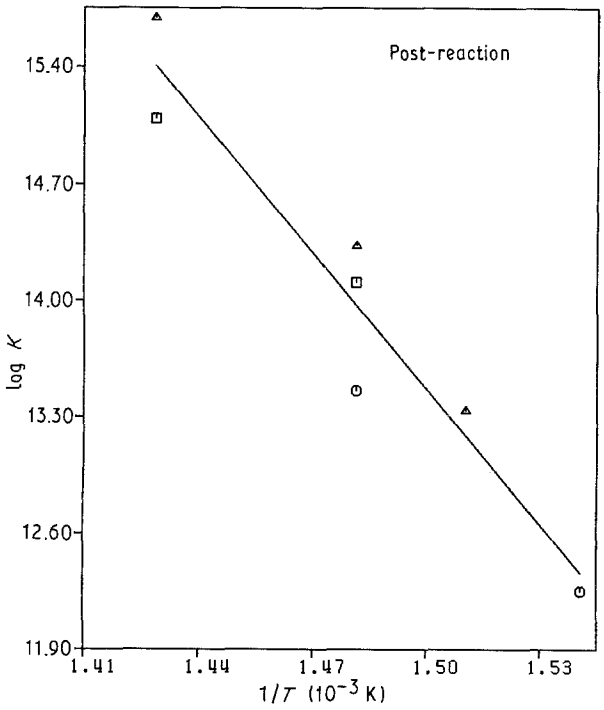

Figure 6 Arrhenius plot for the crystallite coarsening kinetics after reaction. (□) CdO (2 0 0), sample I; (○) CdO (2 2 0); (△) CdO (1 1 1).

evaporation–condensation kinetics remains reasonable. During the reaction the average of n is 4.2 $\pm$ 0.2, consistent with surface diffusion. Notice that the average is raised from 4.0_5 by the single value of 4.5 for the CdO (2 0 0) plane at 675 K for the second sample. The kinetics of decomposition and particle growth have been shown to be dependent on the sample [3]. Also, the anomalous value for CdO (2 2 0) at 649 K is resolved, the previous low value being the result of the significant imperfection profile broadening at low temperatures. After the growth plateau, the results are probably not reliable, the value of n being 5.8 and 2.5 for the CdO (2 2 0) plane at 675 and 649 K, respectively. However, high values of n have been observed near the end of the reaction in other calcination studies [4].

From Equation 4 the rate constant, k, can be found for coarsening during the reaction (n = 4) and after the reaction (n = 3.3). During the reaction, strain broadening increases the rate constant by a factor of $\sim$2. From the Arrhenius plot (Fig. 5), it is seen that the rate constants for growth may be different for the two planes during reaction, reflecting the difference in the surface diffusion coefficient. This is at odds with the results from Equation 1, and needs to be examined further. For the CdO (2 0 0) plane, this gives an activation energy of $\sim$138 kJ mol^{-1}, close to the value obtained from Equation 1.

The rate constants after the reaction are about two orders of magnitude less than during the reaction. From the Arrhenius plot (Fig. 6) the coarsening is seen to be the same for all planes. The activation energy is larger than that from Equation 1, and not the same as during the reaction, being $\sim$226 kJ mol^{-1}.

It is worthwhile to compare the results here with those of Nan [4]. Nan divided sintering during the calcination of $MgCO_3$ into three stages: (1) adjustment of structure and a small sintering exponent, (2) a process of little shrinkage of aggregates with particle growth by evaporation–condensation and surface diffusion, (3) a process with considerable shrinkage, with crystallite growth by volume diffusion and/or grain-boundary diffusion, and with a large sintering exponent. The results from this study are consistent with Nan's stage 2, but we have observed an induction period for growth instead of stage 1 and no period corresponding to stage 3. The reasons for the first difference have been discussed, and the second may be due to the relatively higher vapour pressure of CdO compared to MgO, leading to a greater mass transport by evaporation–condensation. If this is true, then evaporation–condensation for small particles is the predominant mass-transport mechanism and it is not appropriate to describe this as the rate-determining step.

In spite of the above considerations, the kinetics expressed earlier by Equation 1, still provide a description of the growth and should not be discounted. Indeed, we have found that growth during calcination of $MgCO_3$ as determined from Nan's plot [4] fits Equation 1 quite well. Elsewhere we derive an expression for recrystallization in powder compacts during decomposition that reduces to Equation 1. Recrystallization serves well to account for the loss of imperfections.

Finally, we point out that Nan's data show a large value of n for stage 3 ($\sim$10) and for our data there is a brief induction period, which may correspond to stage one. It may be commented that there may be difficulty with applying sintering theory to powder compacts of a material sintering in a matrix. A more appropriate model, at least early in the reaction, may be similar to those for supported catalysts [18]. Dispersion of a high vapour pressure oxide, such as CdO,

over the matrix may be significant and n, as determined from log–log plots, may appear to have a time dependence, often becoming as large as 12. Also, for separated particles and aggregates, nucleation-inhibited growth by evaporation–condensation may be a factor [19].

4. Conclusion

Product particle growth during and after a reaction are kinetically controlled by different mechanisms. In terms of particle coarsening, the data indicates that growth during a reaction is kinetically controlled by surface diffusion, but after a reaction by evaporation–condensation. There are several factors that account for the change in mechanism, including the presence of CO_2 and a parent-phase matrix during decomposition.

There are four periods of growth during reaction. (1) The early reaction stage, in which coarsening is very slow and the density of crystal imperfections is high [3]. The product particles and/or aggregate are separated by the parent-phase matrix, and the product particle size is dominated by the rate of formation of CdO by activation. The particles are the most reactive at this stage. (2) An intermediate reaction stage coarsening, for which particle size increases by surface diffusion, although this may be only the rate-determining step. The density of imperfections is decreasing [3], and the sample is losing its reactivity. The surface area is increasing. (3) Late reaction stage coarsening, for which the rate of coarsening is decreasing and the rate-controlling mechanism is changing to evaporation–condensation. The surface are may begin to decrease. The CdO is becoming well annealed, and resembling, for sintering considerations, an oxide powder compact. At this stage, the decomposition rate laws may begin to fail and the back reaction may be retarded. This stage may be marked by retention and may determine the reversibility of the reaction (4), an early product stage, or the usual initial stage tering of powders of small particle size. There may be some residual strain [3], but the reactivity of the powder is expected to decrease with further heat treatment as the surface area decreases.

At different localities in the specimen, different stages may be reached at different times, depending upon the development of the product-phase aggregates.

References

1. C. N. R. RAO, J. GOPALAKRISHNAN, K. VIDYUSAGAR, A. K. GANGULI, A. RAMANAN and L. GANAPATHI, *J. Mater. Res.* **1** (1986) 280.
2. E. RUCKENSTEIN, S. NARAIN and NAE-LIH WU, *ibid.* **4** (1989) 267.
3. J. R. SCHOONOVER and S. H. LIN, *J. Solid State Chem.* **78** (1988) 143.
4. LI NAN, *J. Mater. Sci.* **24** (1989) 485.
5. J. R. SCHOONOVER and S. H. LIN, unpublished results (1989).
6. T. QUADIR and D. W. READY, *J. Amer. Ceram. Soc.* **69** (1986) C-15.
7. G. GRESKOVICH and K. W. LAY, *ibid.* **55** (1972) 142.
8. A. J. C. WILSON, "X-ray Optics", 2nd Edn (Methuen, London, 1962).
9. J. I. LANGFORD, *J. Appl. Crystallogr.* **15** (1982) 315.
10. J. I. LANGFORD and A. J. C. WILSON, in "Crystallography and Crystal Perfection", edited by G. N. Ramochandron (Academic, New York, 1963) p. 207.
11. H. P. KLUG and L. E. ALEXANDER, "X-ray Diffraction Procedures", 2nd Edn (Wiley, New York, 1974).
12. J. I. LANGFORD and A. J. C. WILSON, *J. Appl. Crystallogr.* **11** (1978) 102.
13. C. HERRING, *J. Appl. Phys.* **21** (1950) 301.
14. G. L. MESSING, A. R. SELCUKER and R. C. BRADT, in "Sintering and Heterogeneous Catalysis" edited by G. C. Kuczynski, A. E. Miller and G. A. Sargent (Plenum, New York, 1984) p. 329.
15. G. C. KUCZYNSKI, *Met. Trans. AIME* **185** (1949) 169.
16. D. BERUTO, R. BUTTER and A. W. SEARCY, *J. 30Amer. Ceram. Soc.* **67** (1984) 512.
17. J. R. SCHOONOVER and S. H. LIN, *Mater. Lett.* **7** (1988) 274.
18. E. RUCKENSTEIN, in "Metal Support Interactions in Catalysis, Sintering, and Redispersion", edited by S. A. Stevenson, J. A. Dumesic, R. T. K. Baker and E. Ruckenstein (Van Nostrand Reinhold, New York, 1987) p. 139.
19. P. WYNBLATT and N. A. GJOSTEIN, *Prog. Solid State Chem.* **9** (1974) 21.

Received 23 May
and accepted 23 October 1989